Synthesis, Hole Doping, and Electrical Properties of a Semiconducting Azatriangulene-Based Covalent Organic Framework

David W. Burke,[‡1] Raghunath R. Dasari,[‡2] Vinod K. Sangwan,[3] Alexander K. Oanta,[1] Zoheb Hirani,[1] Chloe E. Pelkowski,[1,2] Yongjian Tang,[4] Ruofan Li,[4] Daniel C. Ralph,[4] Mark C. Hersam,[1,3] Stephen Barlow,[2,5] Seth R. Marder,[2,5,6*] and William R. Dichtel[1,*]

[1] Department of Chemistry, Northwestern University, Evanston, Illinois 60208, USA

[2] School of Chemistry and Biochemistry, Georgia Institute of Technology, Atlanta, Georgia 30332, USA

[3] Department of Materials Science and Engineering, Northwestern University, Evanston, Illinois 60208, USA

[4] Department of Physics, Cornell University, Ithaca, New York 14853, USA

[5] Renewable & Sustainable Energy Institute, University of Colorado Boulder, Boulder, Colorado 80303, USA

[6] Departments of Chemistry and of Chemical and Biological Engineering, University of Colorado Boulder, Boulder, Colorado 80309, USA

[‡] Authors contributed equally to this work

ABSTRACT: Two-dimensional covalent organic frameworks (2D COFs) containing heterotriangulenes have been theoretically identified as semiconductors with tunable, Dirac-cone-like band structures, which are expected to afford high charge-carrier mobilities ideal for next-generation flexible electronics. However, few bulk syntheses of these materials have been reported, and existing synthetic methods provide limited control of network purity and morphology. Here, we report transimination reactions between benzophenone-imine-protected azatriangulenes (OTPA) and benzodithiophene dialdehydes (BDT), which afforded a new semiconducting COF network, OTPA-BDT. The COFs were prepared as both polycrystalline powders and thin films with controlled crystallite orientation. The azatriangulene nodes are readily oxidized to stable radical cations upon exposure to an appropriate *p*-type dopant, tris(4-bromophenyl)ammoniumyl hexachloroantimonate, after which the network's crystallinity and orientation are maintained. Oriented, hole-doped OTPA-BDT COF films exhibit electrical conductivities of up to 1.2×10^{-1} S cm^{-1}, which are among the highest reported for imine-linked 2D COFs to date.

INTRODUCTION

The discovery of graphene and its extraordinary electronic properties has inspired a surge of interest in the preparation of other two-dimensional (2D) nanomaterials for use in next-generation electronics.[1-5] Pairing ultrahigh charge-carrier mobility[6,7] with excellent tensile strength,[7,8] flexibility,[9] and high thermal conductivity,[10] graphene is well-positioned to become an integral component of circuitry in printable electronics.[9,11,12] Despite these advantages, its zero band gap and limited structural tunability largely preclude its use in most semiconductor-based devices, motivating the search for analogous 2D materials with tunable band gaps.[13] Two-dimensional covalent organic frameworks (2D COFs) are an emergent class of crystalline polymers that could fill this gap.[14-16] These materials are prepared by condensing multifunctional monomers into stacks of macromolecular sheets, such that the resulting pore sizes, shapes, and functionality emerge from the monomer structures.[17] By combining planar, conjugated monomers that form tight π-stacks, semiconducting COF networks with tunable band gaps have been prepared,[18-30] which have already shown promise in photovoltaics,[31,32] organic field-effect transistors,[25,30,33] and chemiresistive sensors.[23] Despite this progress, all tested materials exhibit far lower charge-carrier mobility and conductivity values compared to state-of-the-art one-dimensional (1D) conducting polymers due to their nanoscale crystallite sizes, frequent lack of crystallite orientation, disordered grain boundary defects, and poor conjugation within and between monomers, impeding their transition to industrial relevance.[20,34] Chemical doping has been leveraged to introduce additional charge carriers into COFs, thus increasing their electrical conductivity.[20,22,24,27-29,35] However, many studies predominantly examine uncontrolled *p*-type doping with iodine vapor,[22,27,28,35] which presents several complicating factors because of its weak oxidant strength and high volatility.[36,37] Most notably, the high vapor pressure required for doping leads to the accumulation of excess iodine within COF pores and grain boundaries that disperses over time, leading to unstable device performance.[24,37] Hence, the design of new conductive 2D COF materials, as well as the investigation of controlled, liquid-phase doping strategies, remain important frontiers.

Towards this objective, heterotriangulenes have recently attracted substantial interest as COF building blocks, as they are predicted to tile into hexagonal networks exhibiting Dirac-cone-like electronic structures similar to that of graphene, leading to high charge-carrier mobilities and conductivities.[5,38] In particular, azatriangulenes have been targeted due to their greater synthetic accessibility compared to boron and carbon radical-based alternatives.[5,39,40] Azatriangulene-based 2D polymers are predicted to have tunable band gaps (<3 eV) between unfilled flat bands and filled Dirac-cone-like sharp bands that can support hole mobilities of up to 800 cm^2 V^{-1} s^{-1} depending on the chemical structure.[5] Moreover, the electron-rich central amine of some azatriangulenes can be oxidized to a

stable radical cation at moderate potentials, thus enabling charge injection or chemical doping to increase the number of charge carriers.[22] Although the on-surface syntheses of azatriangulene 2D polymers and macrocycles have been reported,[41-43] the first bulk synthesis of an imine-linked azatriangulene COF as a polycrystalline powder was only recently reported by Perepichka and coworkers.[22] This material, composed of a tris(amine) derivative of oxygen-bridged triphenylamine (4,4',4"-triamino-2,2':6',2":6",6-trioxytriphenylamine, OTPA-NH_2) and 2,5-dihydroxyterephthalaldehyde, was compressed into pellets, whose conductivities were measured as prepared (up to 1.6×10^{-5} S cm^{-1}) and after *p*-type doping with iodine (up to 1×10^{-2} S cm^{-1}). While these are among the highest values reported for 2D imine-linked COFs thus far, the authors noted that the OTPA-NH_2 precursor must be generated and consumed exclusively under inert atmosphere, as it undergoes rapid oxidation in air. This sensitivity precluded monomer purification and direct characterization prior to COF synthesis, potentially leading to the incorporation of impurities and defects into the tested materials. In addition, the preparation of azatriangulene-based COF thin films with controlled crystallite orientation has not yet been demonstrated, and uniform orientation may improve electrical conductivity by maximizing contact between crystalline domains.[33] Therefore, new methods to synthesize oriented, crystalline azatriangulene-based COF materials from air-stable precursors are greatly needed.

Here we report the synthesis of a second-generation imine-linked azatriangulene 2D COF, which overcomes the challenges outlined above. In this case, OTPA-NH_2 is paired with a conjugated benzodithiophene dialdehyde (4,8-diethoxybenzo[1,2-*b*:4,5-*b'*]dithiophene-2,6-dicarbaldehyde, BDT, **1**), as it has been shown to better facilitate charge transport in semiconducting COFs compared to more conventional monomers, such as terephthalaldehyde.[24] Moreover, rather than using a crude sample of the air-sensitive OTPA-NH_2 monomer, we use an air-stable equivalent, a benzophenone-imine protected form (OTPA-benzophenone, **2**). **2** is readily accessible using Pd-catalyzed amination reactions and is bench stable, which facilitated its purification. The isolated monomer was then subjected to solvothermal COF polymerization via transimination reactions.[44] The resulting network (OTPA-BDT COF, **Scheme 1**) was prepared in the forms of polycrystalline powders and oriented thin films in one pot, with the latter obtained by submerging an appropriate substrate in the reaction mixture. OTPA-BDT COF thin films were oxidatively doped with tris(4-bromophenyl)ammoniumyl hexachloroantimonate (commonly known as magic blue) while maintaining their crystallinity and orientation. Finally, we measured the electrical conductivity of the thin films before and after doping, revealing reproducible values of up to 1.2×10^{-1} S cm^{-1} after doping depending on film thickness, which, to the best of our knowledge, is one of the highest values reported for an imine-linked 2D COF.[35] Collectively, these results highlight the potential of heterotriangulene COFs as semiconducting materials in next-generation organic electronic devices.

RESULTS AND DISCUSSION

Solvothermal transimination reactions between **1** and **2** afford polycrystalline OTPA-BDT COF powders, which exhibit X-ray diffraction features consistent with the expected hexagonal lattice. To prepare **2**, 4,4',4"-tribromo-2,2':6',2":6",6-trioxytriphenylamine (OTPA-Br) was first synthesized by following previously reported protocols,[39, 40] then elaborated with three benzophenone imines via a Buchwald-Hartwig amination reaction.[45] The resulting monomer was heated in the presence of **1**, acetic acid, and a 4:1 *v*/*v* 1,4-dioxane/mesitylene mixture under nitrogen atmosphere, resulting in the precipitation of black OTPA-BDT COF powder in 5 days (**Scheme**

Scheme 1. Synthesis of OTPA-BDT COF via transimination reactions

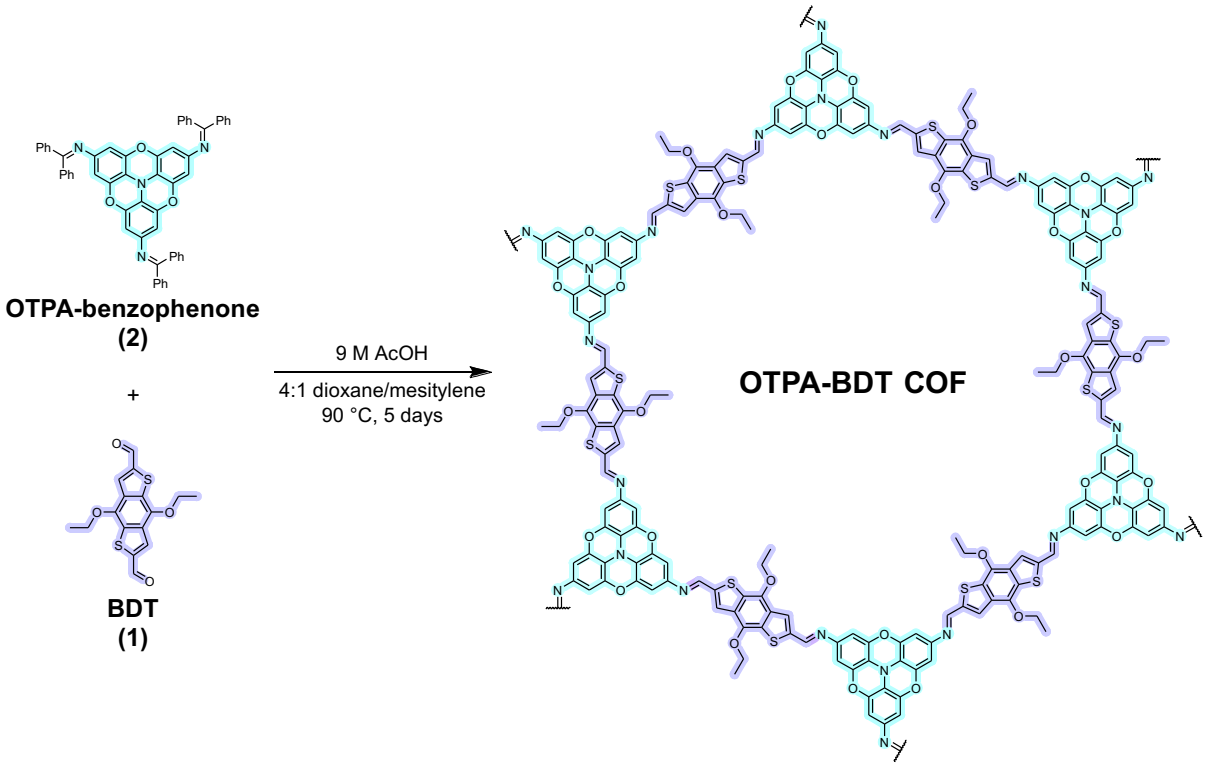

1, see Supporting Information for synthetic procedures). These powders were washed with methanol and activated by supercritical CO_2 drying prior to characterization by powder X-ray diffraction (PXRD) and infrared (IR) spectroscopy (**Figure 1**). PXRD measurements of OTPA-BDT COF powder reveal the presence of four sharp diffraction features at 2θ values of less than 10°, which are consistent with a typical 2D COF diffraction pattern. To assign these peaks and confirm the COF structure, a model of the targeted network was constructed and refined (Pawley method) against the experimental pattern (see Supporting Information for details). The Pawley-refined model (**Figure 1A**) exhibits a simulated PXRD pattern that agrees (R_P = 2.96, R_{WP} = 3.99) with the experimental data (**Figure 1B**), indicating that the synthesized materials are well-represented by a hexagonal unit cell with eclipsed stacking (a = b = 37.98 Å, c = 3.31 Å, α = β = 90°, γ = 120°). According to this analysis, the peaks at 2θ = 2.7°, 4.7°, 5.4°, and 7.2° can be assigned to the (100), (110), (200), and (210) planes, respectively. We note that this model may oversimplify the network's true interlayer stacking behavior, as 2D COF PXRD patterns include few if any out-of-plane reflections that can be used to distinguish subtle differences in packing. Moreover, recent single-crystal electron-diffraction measurements of multiple common 2D COF networks suggest the presence of more complex packing arrangements.[46,47] In addition, IR spectroscopy of the COF powder reveals a sharp imine stretch at 1610 cm^{-1}, confirming the formation of the desired linkages (**Figure 1C**). Thermogravimetric analysis (TGA) of the COF powder suggests that bulk decomposition of the network occurs between 250 and 400 °C (**Figure S1**). We note that upon formation of the COF lattice, the OTPA nodes become sensitized to oxidation by atmospheric oxygen. This results in the inadvertent *p*-type doping of the OTPA-BDT COF over time when stored in air, as confirmed by electron paramagnetic resonance (EPR) spectroscopy (**Figure S2**). Therefore, all OTPA-BDT COF materials discussed from this point forward were stored under a nitrogen atmosphere immediately after the workup, unless otherwise noted. Collectively, these data strongly support the formation of the targeted OTPA-BDT COF lattice.

Polymerizing **1** and **2** in the presence of flat substrates results in the deposition of OTPA-BDT COF thin films onto their surfaces, with crystallite orientation defined by the reaction conditions and choice of substrate. To facilitate conductivity measurements, we explored thin-film growth on non-conductive sapphire substrates with atomically flat surfaces, which contain sparsely and regularly-spaced prepatterned pairs of gold electrodes (channel length = 2 μm, **Figure S15**).[18] When this substrate was submerged in the optimized COF powder reaction mixture described above, a continuous, purple film formed over the surface of the sapphire substrate and gold contacts (see Supporting Information for a detailed procedure). Grazing-incidence wide-angle X-ray scattering (GIWAXS) measurements of these films (**Figure 2B**) reveal several bright diffraction features at q < 1.0 $Å^{-1}$, with intensity localized along q_y, which agree with the predicted in-plane diffraction features of the OTPA-BDT COF. Likewise, the bright feature at q > 1.5 $Å^{-1}$, with greater intensity along q_z, is assigned to the consistent interlayer spacing between

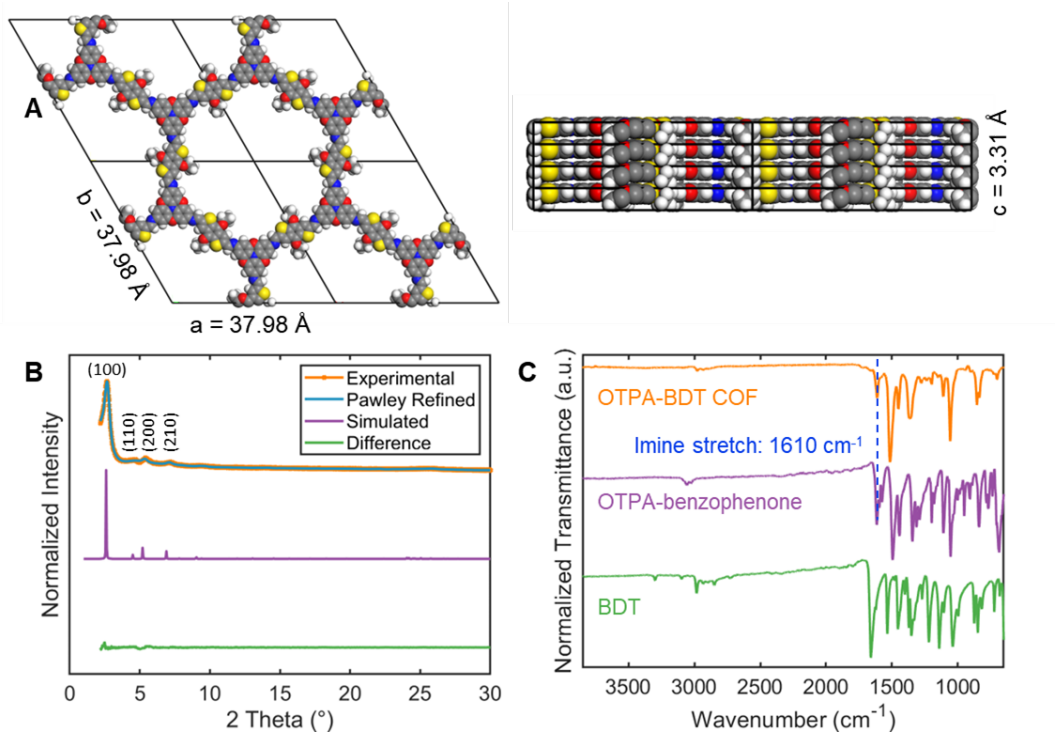

Figure 1. (A) Top-down (left) and side-on (right) views of the OTPA-BDT COF model after Pawley refinement. (B) An experimental PXRD pattern of OTPA-BDT COF powder (orange) is in excellent agreement with a Pawley-refined simulation (blue) as indicated by the limited difference between the two (green), suggesting that the model in (A) accurately represents the lattice structure of the prepared materials. A simulated PXRD pattern of the geometry optimized OTPA-BDT COF model before Pawley refinement (purple) is plotted alongside them for reference. (C) IR spectra of OTPA-BDT COF powder, OTPA-benzophenone, and BDT. Both the COF powder and OTPA-benzophenone monomer produce sharp peaks at approximately 1610 cm^{-1}, indicating that these materials contain the expected imine linkages.

π-stacked COF sheets. The anisotropic intensity of in-plane and out-of-plane signals indicates that COF layers are preferentially oriented parallel to the sapphire surface. This arrangement may facilitate charge transport by minimizing gaps between crystallites.[35] Although a recent study reported only subtle differences in electrical conductivity between moderately oriented COF films and unoriented powder pellets, the anisotropy is expected to be higher in highly conducting COF films.[24] Atomic force microscopy (AFM) measurements suggest that the films are reasonably smooth (rms roughness, $Rq \leq 25$ nm), with mean thicknesses of 170-190 nm measured for three separately prepared films (**Figures S3** and **S13B**), although we note that residual powder byproducts are scattered across the surface in all cases. Scanning electron microscopy (SEM) images of the film surface further corroborate the surface morphology observed by AFM (**Figure S4**). Films with greater preferential crystallite orientation can be prepared by exchanging sapphire substrates for silicon-supported monolayer graphene (**Figure S5**), which templates COF growth through π-stacking,[48] but graphene's high conductivity precludes its use in experiments designed to evaluate the intrinsic electronic properties of the COF layer. Alternatively, polymerization in 1:1 *v*/*v* *o*-dichlorobenzene/*n*-butanol affords OTPA-BDT COF films on patterned sapphire with equivalent crystallinity but no preferential orientation (**Figure S6**, see Supporting Information for synthetic protocol). Collectively, these results demonstrate the formation of OTPA-BDT COF thin films with tunable crystallite orientation, which will facilitate the comprehensive characterization of their electronic properties.

OTPA-BDT COF thin films can be doped with holes (*p*-type doping) via exposure to magic blue while maintaining their long-range order and crystallite orientation. Hole doping is a convenient way to incorporate additional charge carriers into oxidizable COF networks, thus increasing their electrical conductivities. Although most studies thus far have used iodine vapor for this purpose,[35] the lack of stoichiometric control and unstable device performance afforded by this method[23,24] motivated us to develop a solution-phase doping protocol involving a stronger dopant for OTPA-BDT COF materials (**Figure 2A**). Magic blue was identified as a suitable dopant because it has been shown to provide controlled and stable *p*-type doping for other materials,[49,50] and because of its reduction potential (+0.7 V vs. $FeCp_2^{+/0}$ in CH_2Cl_2),[51] making it a sufficiently powerful and stable oxidant for OTPA's electron-rich central amine (the oxidation potential for 2,2':6',2'':6'',6-trioxytriphenylamine is +0.20 V vs. $FeCp_2^{+/0}$ in CH_2Cl_2, see **Figure S7**). To test this dopant, pristine OTPA-BDT COF powder was first soaked in a dichloromethane solution of magic blue under nitrogen atmosphere, then washed with fresh solvent to remove the excess dopant (see Supporting Information for detailed procedures). After drying in a nitrogen atmosphere, the powder was characterized by EPR spectroscopy, revealing the emergence of a strong signal consistent with the oxidation of the OTPA nodes to stable radical cations (**Figure S8**). Monomer **2** is also oxidized upon incubation with magic blue,

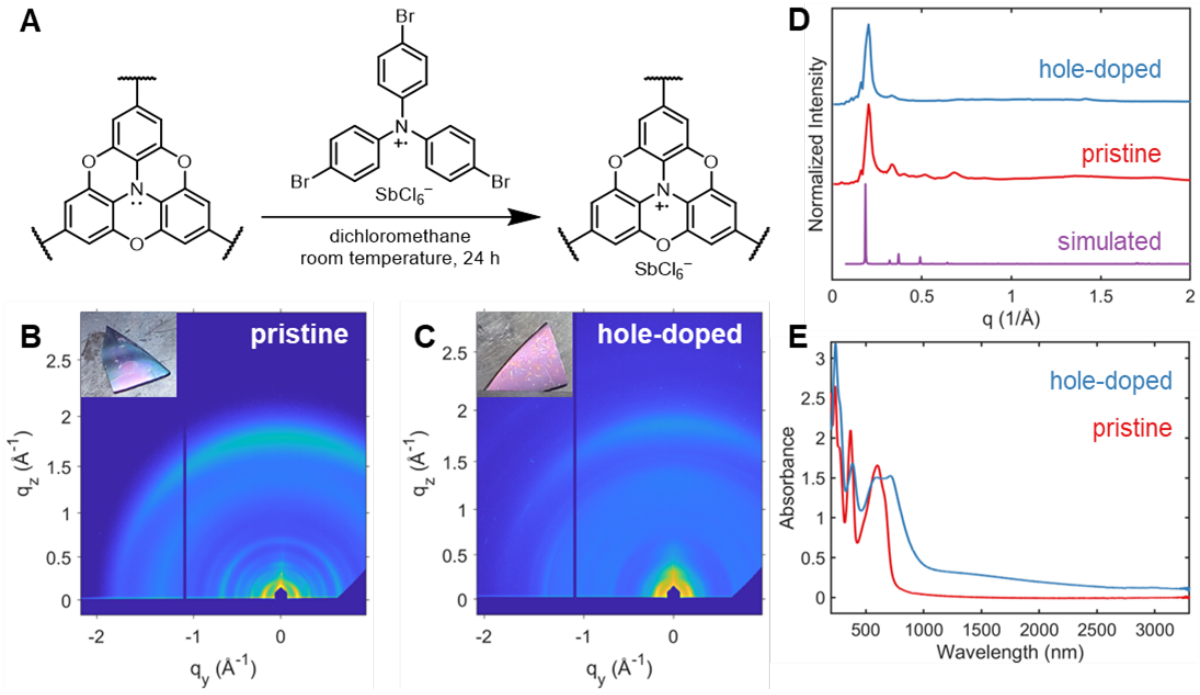

Figure 2. (A) Schematic of the doping protocol for OTPA-BDT COF, in which magic blue oxidizes the central amine of the OTPA nodes to a stable radical cation. (B) GIWAXS pattern and photograph of a pristine, moderately oriented OTPA-BDT COF thin film on patterned sapphire. (C) GIWAXS pattern of the same film after exposure to magic blue reveals that its crystallinity and orientation are maintained upon doping. Inset: A photograph of the film surface reveals a slight color change after doping. (D) Horizontal linecuts of the GIWAXS patterns in (B) and (C) ($0° \leq \phi \leq 10°$), which showcase their in-plane diffraction features, are in good agreement with a simulated diffraction pattern of the geometry optimized OTPA-BDT COF model prior to Pawley refinement (purple), indicating that the films exhibit the intended crystal structure. (E) UV-Vis absorption profile for an OTPA-BDT COF thin film grown on sapphire before (red) and after (blue) *p*-type doping with magic blue, plotted as a function of wavelength. The absorption profile is red-shifted upon oxidation of the azatriangulene nodes.

as verified by EPR measurements (**Figure S9**). With appropriate doping conditions identified, the same protocol was then applied to an oriented OTPA-BDT COF thin film on patterned sapphire. The film became subtly darker in color after soaking in the magic blue solution, providing a first indication of successful oxidation. UV-Vis spectroscopy measurements of the film reveal that the COF absorption profile is red-shifted and extends into the near-IR (>900 nm) after exposure to magic blue (**Figures 2E** and **S10**), as expected for the formation of triarylamine radical cations.[52] There is also an increased absorbance in the mid-IR (up to 3300 nm) likely arising from intervalence transitions induced by doping. GIWAXS measurements (**Figure 2B-D**) indicate that the COF film retains its signature diffraction features and crystallite orientation after doping. Notably, the relative intensity of the (100) diffraction signal increased with respect to the higher-order peaks, which may be due to the incorporation of $SbCl_6^-$ counterions into the oxidized COF lattice. Identical behavior was observed upon exposure of an unoriented OTPA-BDT COF film to magic blue (**Figure S6**). To further confirm the successful oxidation of the azatriangulene nodes with magic blue, the compositions of pristine and *p*-type doped OTPA-BDT COF films were probed by X-ray photoelectron spectroscopy (XPS). Prior to doping, the film exhibited only carbon, nitrogen, oxygen, and sulfur peaks, as expected for the OPTA-BDT COF network (**Figure S11**). Exposing this pristine film to magic blue resulted in the emergence of additional strong antimony and chlorine peaks (**Figure S12**), consistent with the $SbCl_6^-$ counterion incorporation into the oxidized COF lattice. A weak bromine signal was also observed, suggesting that a small quantity of residual dopant, or the corresponding neutral tris(4-bromophenyl)amine byproduct, remains adsorbed to the surface of the film or in its pores after solvent washing, although this is predicted to have minimal impact on the electrical properties of the COF film. Taken together, these findings are consistent with magic blue acting as a *p*-type dopant for the OTPA-BDT COF, as expected based on electrochemical potentials.

Electrical conductivity measurements of an oriented OTPA-BDT COF film reveal a moderate intrinsic conductivity on par with other semiconducting COFs,[35] which increases by almost five orders of magnitude upon *p*-type doping with magic blue. To investigate bulk conductivity, we performed two-probe current-voltage (*I-V*) measurements with an oriented OTPA-BDT COF thin film grown on sapphire-supported gold electrodes (190 nm thick, **Figures S13, S15**). The device shows ohmic behavior at low biases (V < 5 V) before and after doping, enabling the straightforward extraction of bulk conductivity. As-grown pristine COF films show a value ($7.1 \pm 1.0 \times 10^{-7}$ S cm^{-1}) similar to other undoped semiconducting COFs (**Figure 3A-B**), as anticipated given the low expected charge-carrier

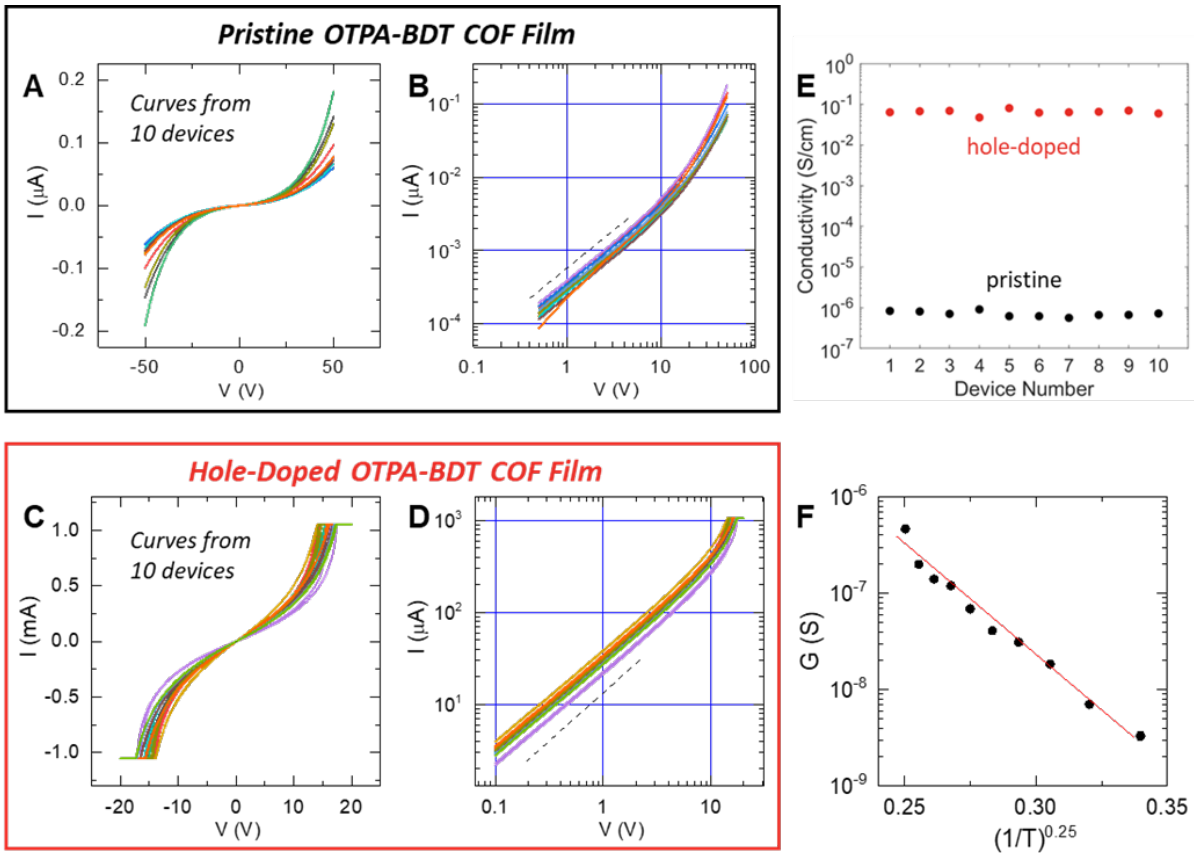

Figure 3. (A) Current-voltage (*I-V*) curves measured across 10 separate pairs of gold electrodes beneath a single, pristine OTPA-BDT COF thin film, each represented by a different color. (B) A log-log plot of the *I-V* curves shown in (A) reveals that current increases linearly as a function of voltage below 5 V, as indicated by the straight dotted line, demonstrating ohmic contacts. (C) *I-V* curves measured across the same 10 devices from (A) after doping the OTPA-BDT COF film with magic blue. (D) A log-log plot of the *I-V* curves from (C) displays linear behavior below 10 V, suggesting that ohmic contacts are maintained after doping. (E) Bulk conductivity values for 10 devices before and after doping the COF layer. (F) Temperature-dependent conductance ($G = I/V$) of a doped device (black) is in excellent agreement with a 3D variable range hopping model (red). Corresponding *I-V* curves for different temperatures are shown in **Figure S17**.

concentrations.[35] On the other hand, the bulk conductivity of the COF film after doping was 6.5 ± 0.8 × 10^{-2} S cm^{-1}, which is one of the highest measured values for 2D imine-linked COFs (**Figure 3C-E**).[35]

Conductivities measured from ten distinct electrode pairs over the ~1 cm^2 area chip suggested good uniformity of the COF film and doping levels (**Figure 3E**).[18] The *I-V* characteristics become superlinear ($I \sim V^{2.5}$) at high biases (> 10 V), which can be explained by space-charge limited current (SCLC) and trap-limited processes.[53-55] While $I \sim V^m$ behavior with $m = 2$ is commonly seen in organic semiconductors, $m > 2$ is also widely observed in bulk materials, where the coefficient m depends on trap density of states.[56] Nonlinearity in *I-V* curves can also be attributed in part to internal thermal heating in the devices that increases their bulk conductivity in a positive feedback manner, but these devices do not show any hysteretic loop, suggesting that this is not the primary mechanism.[57] The doped devices reach current compliance (1 mA) at 14 - 16 V. If the current compliance is increased to 10 mA or higher, the devices undergo catastrophic breakdown, which is likely due to excessive heating in the channel. To evaluate the performance stability of the doped COF film, the same film was remeasured after storage in a nitrogen glovebox for 8 months, revealing a 50-fold reduction in electrical conductivity (1.2 × 10^{-3} S cm^{-1}) compared to the freshly doped sample (**Figure S16**). This decrease in conductivity may be indicative of some degree of chemical degradation of the doped network during extended storage. We note that iodine-doped COF networks have been reported to undergo an equivalent loss of conductivity in as little as 24 hours after doping,[23, 24] highlighting the superior performance stability afforded by our liquid-phase doping protocol. The underlying charge-transport mechanism in the doped COF film was further investigated via variable-temperature conductivity measurements. Low-bias conductivity was found to be in excellent agreement with a three-dimensional variable range hopping (3D VRH) model, given by $\sigma(T) = \sigma_0 \exp\left[{}^{T_0}/_{T}\right]^{-0.25}$ (**Figure 3F**).[58] 3D VRH charge transport can be expected for these COF films, where mobile carriers are largely localized within individual nanocrystalline domains or within even smaller regions depending on the localization length.[36] This finding suggests that further chemical modifications should aim to delocalize the carrier state to attain band-like transport for high conductivity and field-effect mobility in COF-based electronic devices.

Electrical conductivity measurements for OTPA-BDT COF devices with variable interelectrode distances reveal consistent conductivity values across all tested channel lengths and enable the calculation of contact resistance. To evaluate the impact of interelectrode distance on the measured conductivity values of OTPA-BDT COF thin films, a pristine film was grown on the surface of a sapphire substrate prepatterned with pairs of gold electrodes exhibiting variable channel lengths of 1-16 μm. In this case, the COF layer grew to a thickness of 430 nm, as verified by AFM (**Figure S14**). *I-V* measurements demonstrate that the resistance of the pristine COF film increases linearly as a function of channel length, corresponding to a consistent, moderate conductivity of 8.3 × 10^{-5} S cm^{-1} (**Figure S18**) for the pristine devices. After hole-doping with magic blue, the film conductivity increased to 1.2 × 10^{-1} S cm^{-1}, with device resistance still scaling linearly based on channel length (**Figure S19-20**). We note that the measured conductivity values for this film (430 nm thick) are higher than those observed for the 190 nm thick film (**Figure 3**) before and after *p*-type doping, which may be due to improved percolating effects in the thicker film. By extrapolating the linear fit of the resistance versus channel length curve (**Figure S20**), a contact resistance of 5.91 kΩ was calculated for the doped COF devices. This resistance corresponds to a width normalized value of 14.8 Ω-cm, indicating good ohmic electrical contact between the COF layer and gold electrodes. The reproducibly high conductivity values highlight the excellent quality of the OTPA-BDT COF thin films, as well as their potential for use in semiconductor-based devices.

CONCLUSION

Polycrystalline powders and thin films of the new azatriangulene-based OTPA-BDT COF were prepared and characterized. By selecting appropriate polymerization conditions and substrates, thin films with tunable crystallite orientation were prepared, which should facilitate future investigations into the influence of orientation on fundamental electronic properties. Solution-phase *p*-type doping with magic blue oxidized the OTPA nodes to the corresponding radical cations while maintaining bulk network crystallinity. Finally, oriented thin films of hole-doped OTPA-BDT COF were found to exhibit electrical conductivities of up to 1.2 × 10^{-1} S cm^{-1} depending on film thickness, which is among the highest values reported for 2D imine-linked COFs to date. These results highlight the potential of designed 2D polymers to function as high-performance semiconductors, but they also demonstrate the need for further improvements in COF materials quality to ensure that their intrinsic properties are measured and ultimately leveraged in electronic devices. Despite our best synthetic efforts and choice of monomers, these materials still exhibit electrical conductivities well below state-of-the-art doped 1D polymers (>10^3 S cm^{-1}), perhaps because a high density of grain boundaries between nanoscale crystallites impedes charge transport.[35, 36] By prioritizing the formation of much larger crystalline domains in future materials, semiconducting COFs with macroscopic charge carrier mobilities rivaling or exceeding those of 1D polymers might be prepared, which would accelerate the realization of sophisticated electronic devices based on flexible organic macromolecules.

ASSOCIATED CONTENT

The Supporting Information is available free of charge on the ACS Publications website.

Materials, instrumentation, synthetic protocols for OTPA-BDT COF monomers and materials, description of electrical conductivity measurements, and additional COF characterization data (PDF)

Pawley-refined model of OTPA-BDT COF (CIF)

AUTHOR INFORMATION

Corresponding Authors

* William R. Dichtel – wdichtel@northwestern.edu
* Seth R. Marder – seth.marder@colorado.edu

ORCID

David W. Burke: 0000-0002-4517-2178
Raghunath R. Dasari: 0000-0002-3237-7334
Vinod K. Sangwan: 0000-0002-5623-5285
Alexander K. Oanta: 0000-0002-3188-2240
Ruofan Li: 0000-0001-7746-9569
Daniel C. Ralph: 0000-0002-3026-0335

Mark C. Hersam: 0000-0003-4120-1426
Stephen Barlow: 0000-0001-9059-9974
Seth R. Marder: 0000-0001-6921-2536
William R. Dichtel: 0000-0002-3635-6119

Author Contributions

‡D.W.B. and R.R.D. contributed equally to this work, and their names are listed alphabetically.

Notes

The authors declare no competing financial interests.

ACKNOWLEDGMENT

This work was supported by the Army Research Office in the form of a Multidisciplinary University Research Initiatives (MURI) award under grant number W911NF-15-1-0447. Z.H. is supported by the NSF Graduate Research Fellowship Program under grant number DGE-1842165. This work made use of the IMSERC Crystallography and Physical Characterization facilities at Northwestern University, which have received support from the Soft and Hybrid Nanotechnology Experimental (SHyNE) Resource (NSF ECCS-2025633) and Northwestern University, as well as the SPID facility of Northwestern University's NUANCE Center, which has received support from the SHyNE Resource (NSF ECCS-2025633), the IIN, and Northwestern's MRSEC program (NSF DMR-1720139). V.K.S. and M.C.H. acknowledge the support from Northwestern University Materials Research Science and Engineering Center (MRSEC) (NSF DMR-1720139). Y.T. acknowledges support by the DOE (DE-SC0017671). This work was performed in part at the Cornell NanoScale Facility, an NNCI member supported by NSF Grant NNCI-2025233. Portions of this research were performed at Sector 8-ID-E of the Advanced Photon Source, a U.S. Department of Energy (DOE) Office of Science user facility operated for the DOE Office of Science by Argonne National Laboratory under Contract No. DE-AC02-06CH11357. This research used resources available at Beamline 11-BM (Complex Materials Scattering) of the National Synchrotron Light Source II, a U.S. Department of Energy (DOE) Office of Science User Facility operated for the DOE Office of Science by Brookhaven National Laboratory under Contract No. DE-SC0012704. D.W.B. and Z.H. thank Drs. Joseph Strzalka, Zhang Jiang, and Ruipeng Li for their assistance with collecting synchrotron X-ray scattering data. S.R.M and R.R.D. thank Dr. Robert Braga for collecting EPR data.

ABBREVIATIONS

COF, covalent organic framework; **OTPA**, oxygen-bridged triphenylamine (2,2':6',2":6",6-trioxytriphenylamine); **OTPA-Br**, 4,4',4"-tribromo-2,2':6',2":6",6-trioxytriphenylamine; **OTPA-NH_2**, 4,4',4"-triamino-2,2':6',2":6",6-trioxytriphenylamine; **OTPA-benzophenone**, *N*-Aryl Benzophenone Imine of 4,4',4"-triamino-2,2':6',2":6",6-trioxytriphenylamine; **BDT**, 4,8-diethoxybenzo[1,2-*b*:4,5-*b'*]dithiophene-2,6-dicarbaldehyde; **OTPA-BDT**, imine-linked COF prepared via transamination reactions between OTPA-benzophenone and BDT.

REFERENCES

(1) Geim, A. K.; Novoselov, K. S. The Rise of Graphene. *Nature Mater.* **2007**, *6*, 183-191.

(2) Novoselov, K. S.; Geim, A. K.; Morozov, S. V.; Jiang, D.; Zhang, Y.; Dubonos, S. V.; Grigorieva, I. V.; Firsov, A. A. Electric Field Effect in Atomically Thin Carbon Films. *Science* **2004**, *306*, 666-669.

(3) Zhang, Y.; Tan, Y.-W.; Stormer, H. L.; Kim, P. Experimental Observation of the Quantum Hall Effect and Berry's Phase in Graphene. *Nature* **2005**, *438*, 201-204.

(4) Novoselov, K. S.; Geim, A. K.; Morozov, S. V.; Jiang, D.; Katsnelson, M. I.; Grigorieva, I. V.; Dubonos, S. V.; Firsov, A. A. Two-Dimensional Gas of Massless Dirac Fermions in Graphene. *Nature* **2005**, *438*, 197-200.

(5) Jing, Y.; Heine, T. Two-Dimensional Kagome Lattices Made of Hetero Triangulenes Are Dirac Semimetals or Single-Band Semiconductors. *J. Am. Chem. Soc.* **2019**, *141*, 743-747.

(6) Chen, J.-H.; Jang, C.; Xiao, S.; Ishigami, M.; Fuhrer, M. S. Intrinsic and Extrinsic Performance Limits of Graphene Devices on SiO2. *Nature Nanotechnol.* **2008**, *3*, 206-209.

(7) Rizzi, L.; Zienert, A.; Schuster, J.; Köhne, M.; Schulz, S. E. Electrical Conductivity Modeling of Graphene-Based Conductor Materials. *ACS Appl. Mater. Interfaces* **2018**, *10*, 43088-43094.

(8) Lee, C.; Wei, X.; Kysar Jeffrey, W.; Hone, J. Measurement of the Elastic Properties and Intrinsic Strength of Monolayer Graphene. *Science* **2008**, *321*, 385-388.

(9) He, P.; Cao, J.; Ding, H.; Liu, C.; Neilson, J.; Li, Z.; Kinloch, I. A.; Derby, B. Screen-Printing of a Highly Conductive Graphene Ink for Flexible Printed Electronics. *ACS Appl. Mater. Interfaces* **2019**, *11*, 32225-32234.

(10) Balandin, A. A.; Ghosh, S.; Bao, W.; Calizo, I.; Teweldebrhan, D.; Miao, F.; Lau, C. N. Superior Thermal Conductivity of Single-Layer Graphene. *Nano Lett.* **2008**, *8*, 902-907.

(11) Berggren, M.; Nilsson, D.; Robinson, N. D. Organic Materials for Printed Electronics. *Nature Mater.* **2007**, *6*, 3-5.

(12) Secor, E. B.; Hersam, M. C. Emerging Carbon and Post-Carbon Nanomaterial Inks for Printed Electronics. *J. Phys. Chem. Lett.* **2015**, *6*, 620-626.

(13) Perepichka, D. F.; Rosei, F. Extending Polymer Conjugation into the Second Dimension. *Science* **2009**, *323*, 216-217.

(14) Côté, A. P.; Benin, A. I.; Ockwig, N. W.; O'Keeffe, M.; Matzger, A. J.; Yaghi, O. M. Porous, Crystalline, Covalent Organic Frameworks. *Science* **2005**, *310*, 1166-1170.

(15) Diercks, C. S.; Yaghi, O. M. The Atom, the Molecule, and the Covalent Organic Framework. *Science* **2017**, *355*, eaal1585.

(16) Evans, A. M.; Strauss, M. J.; Corcos, A. R.; Hirani, Z.; Ji, W.; Hamachi, L. S.; Aguilar-Enriquez, X.; Chavez, A. D.; Smith, B. J.; Dichtel, W. R. Two-Dimensional Polymers and Polymerizations. *Chem. Rev.* **2022**, *122*, 442-564.

(17) Lohse, M. S.; Bein, T. Covalent Organic Frameworks: Structures, Synthesis, and Applications. *Adv. Funct. Mater.* **2018**, *28*, 1705553.

(18) Balch, H. B.; Evans, A. M.; Dasari, R. R.; Li, H.; Li, R.; Thomas, S.; Wang, D.; Bisbey, R. P.; Slicker, K.; Castano, I.; Xun, S.; Jiang, L.; Zhu, C.; Gianneschi, N.; Ralph, D. C.; Brédas, J.-L.; Marder, S. R.; Dichtel, W. R.; Wang, F. Electronically Coupled 2D Polymer/MoS2 Heterostructures. *J. Am. Chem. Soc.* **2020**, *142*, 21131-21139.

(19) Duhović, S.; Dincă, M. Synthesis and Electrical Properties of Covalent Organic Frameworks with Heavy Chalcogens. *Chem. Mater.* **2015**, *27*, 5487-5490.

(20) Evans, A. M.; Collins, K. A.; Xun, S.; Allen, T. G.; Jhulki, S.; Castano, I.; Smith, H. L.; Strauss, M. J.; Oanta, A. K.; Liu, L.; Sun, L.; Reid, O. G.; Sini, G.; Puggioni, D.; Rondinelli, J. M.; Rajh, T.; Gianneschi, N. C.; Kahn, A.; Freedman, D. E.; Li, H.; Barlow, S.; Rumbles, G.; Brédas, J.-L.; Marder, S. R.; Dichtel, W. R. Controlled n-Doping of Naphthalene-Diimide-Based 2D Polymers. *Adv. Mater.* **2022**, 2101932.

(21) Kim, S.; Choi, H. C. Light-Promoted Synthesis of Highly-Conjugated Crystalline Covalent Organic Framework. *Commun. Chem.* **2019**, *2*, 60.

(22) Lakshmi, V.; Liu, C.-H.; Rajeswara Rao, M.; Chen, Y.; Fang, Y.; Dadvand, A.; Hamzehpoor, E.; Sakai-Otsuka, Y.; Stein, R. S.; Perepichka, D. F. A Two-Dimensional Poly(azatriangulene) Covalent Organic Framework with Semiconducting and Paramagnetic States. *J. Am. Chem. Soc.* **2020**, *142*, 2155-2160.

(23) Meng, Z.; Stolz, R. M.; Mirica, K. A. Two-Dimensional Chemiresistive Covalent Organic Framework with High Intrinsic Conductivity. *J. Am. Chem. Soc.* **2019**, *141*, 11929-11937.

(24) Rotter, J. M.; Guntermann, R.; Auth, M.; Mähringer, A.; Sperlich, A.; Dyakonov, V.; Medina, D. D.; Bein, T. Highly Conducting Wurster-Type Twisted Covalent Organic Frameworks. *Chem. Sci.* **2020**, *11*, 12843-12853.

(25) Sun, B.; Zhu, C.-H.; Liu, Y.; Wang, C.; Wan, L.-J.; Wang, D. Oriented Covalent Organic Framework Film on Graphene for Robust Ambipolar Vertical Organic Field-Effect Transistor. *Chem. Mater.* **2017**, *29*, 4367-4374.

(26) Sun, T.; Liang, Y.; Xu, Y. Rapid, Ordered Polymerization of Crystalline Semiconducting Covalent Triazine Frameworks. *Angew. Chem. Int. Ed.* **2022**, *61*, e202113926.

(27) Wang, M.; Wang, M.; Lin, H.-H.; Ballabio, M.; Zhong, H.; Bonn, M.; Zhou, S.; Heine, T.; Cánovas, E.; Dong, R.; Feng, X. High-Mobility Semiconducting Two-Dimensional Conjugated Covalent Organic Frameworks with p-Type Doping. *J. Am. Chem. Soc.* **2020**, *142*, 21622-21627.

(28) Jin, E.; Asada, M.; Xu, Q.; Dalapati, S.; Addicoat Matthew, A.; Brady Michael, A.; Xu, H.; Nakamura, T.; Heine, T.; Chen, Q.; Jiang, D. Two-Dimensional sp2 Carbon–Conjugated Covalent Organic Frameworks. *Science* **2017**, *357*, 673-676.

(29) Cai, S.-L.; Zhang, Y.-B.; Pun, A. B.; He, B.; Yang, J.; Toma, F. M.; Sharp, I. D.; Yaghi, O. M.; Fan, J.; Zheng, S.-R.; Zhang, W.-G.; Liu, Y. Tunable Electrical Conductivity in Oriented Thin Films of Tetrathiafulvalene-Based Covalent Organic Framework. *Chem. Sci.* **2014**, *5*, 4693-4700.

(30) Feldblyum, J. I.; McCreery, C. H.; Andrews, S. C.; Kurosawa, T.; Santos, E. J. G.; Duong, V.; Fang, L.; Ayzner, A. L.; Bao, Z. Few-Layer, Large-Area, 2D Covalent Organic Framework Semiconductor Thin Films. *Chem. Commun.* **2015**, *51*, 13894-13897.

(31) Dogru, M.; Bein, T. On the Road Towards Electroactive Covalent Organic Frameworks. *Chem. Commun.* **2014**, *50*, 5531-5546.

(32) Xu, B.; Li, S.; Jiao, H.; Yin, J.; Liu, Z.; Zhong, W. A Two-Dimensional Quinazoline Based Covalent Organic Framework with a Suitable Direct Gap and Superior Optical Absorption for Photovoltaic Applications. *J. Mater. Chem. A* **2020**, *8*, 3865-3871.

(33) Yue, Y.; Li, H.; Chen, H.; Huang, N. Piperazine-Linked Covalent Organic Frameworks with High Electrical Conductivity. *J. Am. Chem. Soc.* **2022**, *144*, 2873-2878.

(34) Mandal, A. K.; Mahmood, J.; Baek, J.-B. Two-Dimensional Covalent Organic Frameworks for Optoelectronics and Energy Storage. *ChemNanoMat* **2017**, *3*, 373-391.

(35) Souto, M.; Perepichka, D. F. Electrically Conductive Covalent Organic Frameworks: Bridging the Fields of Organic Metals and 2D Materials. *J. Mater. Chem. C* **2021**, *9*, 10668-10676.

(36) Ghosh, R.; Paesani, F. Unraveling the Effect of Defects, Domain Size, and Chemical Doping on Photophysics and Charge Transport in Covalent Organic Frameworks. *Chem. Sci.* **2021**, *12*, 8373-8384.

(37) DeSilva, L. A.; Harwell, J.; Gaquere-Parker, A.; Perera, U. A. G.; Tennakone, K. Thin Films of Copper (I) Iodide Doped with Iodine and Thiocyanate. *Phys. Status Solidi A* **2017**, *214*, 1700520.

(38) Thomas, S.; Li, H.; Bredas, J.-L. Emergence of an Antiferromagnetic Mott Insulating Phase in Hexagonal π-Conjugated Covalent Organic Frameworks. *Adv. Mater.* **2019**, *31*, 1900355.

(39) Kuratsu, M.; Kozaki, M.; Okada, K. 2,2′:6′,2″:6″,6-Trioxytriphenylamine: Synthesis and Properties of the Radical Cation and Neutral Species. *Angew. Chem. Int. Ed.* **2005**, *44*, 4056-4058.

(40) Suzuki, S.; Nagata, A.; Kuratsu, M.; Kozaki, M.; Tanaka, R.; Shiomi, D.; Sugisaki, K.; Toyota, K.; Sato, K.; Takui, T.; Okada, K. Trinitroxide-Trioxytriphenylamine: Spin-State Conversion from Triradical Doublet to Diradical Cation Triplet by Oxidative Modulation of a π-Conjugated System. *Angew. Chem. Int. Ed.* **2012**, *51*, 3193-3197.

(41) Bieri, M.; Blankenburg, S.; Kivala, M.; Pignedoli, C. A.; Ruffieux, P.; Müllen, K.; Fasel, R. Surface-Supported 2D Heterotriangulene Polymers. *Chem. Commun.* **2011**, *47*, 10239-10241.

(42) Steiner, C.; Gebhardt, J.; Ammon, M.; Yang, Z.; Heidenreich, A.; Hammer, N.; Görling, A.; Kivala, M.; Maier, S. Hierarchical On-Surface Synthesis and Electronic Structure of Carbonyl-Functionalized One- and Two-Dimensional Covalent Nanoarchitectures. *Nature Commun.* **2017**, *8*, 14765.

(43) Schlütter, F.; Rossel, F.; Kivala, M.; Enkelmann, V.; Gisselbrecht, J.-P.; Ruffieux, P.; Fasel, R.; Müllen, K. π-Conjugated Heterotriangulene Macrocycles by Solution and Surface-supported Synthesis toward Honeycomb Networks. *J. Am. Chem. Soc.* **2013**, *135*, 4550-4557.

(44) Vitaku, E.; Dichtel, W. R. Synthesis of 2D Imine-Linked Covalent Organic Frameworks through Formal Transimination Reactions. *J. Am. Chem. Soc.* **2017**, *139*, 12911-12914.

(45) Wolfe, J. P.; Åhman, J.; Sadighi, J. P.; Singer, R. A.; Buchwald, S. L. An Ammonia Equivalent for the Palladium-Catalyzed Amination of Aryl Halides and Triflates. *Tetrahedron Lett.* **1997**, *38*, 6367-6370.

(46) Kang, C.; Yang, K.; Zhang, Z.; Usadi, A. K.; Calabro, D. C.; Baugh, L. S.; Wang, Y.; Jiang, J.; Zou, X.; Huang, Z.; Zhao, D. Growing single crystals of two-dimensional covalent organic frameworks enabled by intermediate tracing study. *Nature Commun.* **2022**, *13*, 1370.

(47) Natraj, A.; Ji, W.; Xin, J.; Castano, I.; Burke, D. W.; Evans, A. M.; Strauss, M. J.; Ateia, M.; Hamachi, L. S.; Gianneschi, N. C.; Alothman, Z. A.; Sun, J.; Yusuf, K.; Dichtel, W. R. Single-Crystalline Imine-Linked Two-Dimensional Covalent Organic Frameworks Separate Benzene and Cyclohexane Efficiently. *J. Am. Chem. Soc.* **2022**, *144*, 19813-19824.

(48) Colson, J. W.; Woll, A. R.; Mukherjee, A.; Levendorf, M. P.; Spitler, E. L.; Shields, V. B.; Spencer, M. G.; Park, J.; Dichtel, W. R. Oriented 2D Covalent Organic Framework Thin Films on Single-Layer Graphene. *Science* **2011**, *332*, 228-231.

(49) Tarasov, A.; Zhang, S.; Tsai, M.-Y.; Campbell, P. M.; Graham, S.; Barlow, S.; Marder, S. R.; Vogel, E. M. Controlled Doping of Large-Area Trilayer MoS2 with Molecular Reductants and Oxidants. *Adv. Mater.* **2015**, *27*, 1175-1181.

(50) Tsai, M.-Y.; Zhang, S.; Campbell, P. M.; Dasari, R. R.; Ba, X.; Tarasov, A.; Graham, S.; Barlow, S.; Marder, S. R.; Vogel, E. M. Solution-Processed Doping of Trilayer WSe2 with Redox-Active Molecules. *Chem. Mater.* **2017**, *29*, 7296-7304.

(51) Connelly, N. G.; Geiger, W. E. Chemical Redox Agents for Organometallic Chemistry. *Chem. Rev.* **1996**, *96*, 877-910.

(52) Barlow, S.; Risko, C.; Odom, S. A.; Zheng, S.; Coropceanu, V.; Beverina, L.; Brédas, J.-L.; Marder, S. R. Tuning Delocalization in the Radical Cations of 1,4-Bis[4-(diarylamino)styryl]benzenes, 2,5-Bis[4-(diarylamino)styryl]thiophenes, and 2,5-Bis[4-(diarylamino)styryl]pyrroles through Substituent Effects. *J. Am. Chem. Soc.* **2012**, *134*, 10146-10155.

(53) Lampert, M. A. Simplified Theory of Space-Charge-Limited Currents in an Insulator with Traps. *Phys. Rev.* **1956**, *103*, 1648-1656.

(54) Rose, A. Space-Charge-Limited Currents in Solids. *Phys. Rev.* **1955**, *97*, 1538-1544.

(55) Sangwan, V. K.; Kang, J.; Lam, D.; Gish, J. T.; Wells, S. A.; Luxa, J.; Male, J. P.; Snyder, G. J.; Sofer, Z.; Hersam, M. C. Intrinsic Carrier Multiplication in Layered Bi2O2Se Avalanche Photodiodes with Gain Bandwidth Product Exceeding 1 GHz. *Nano Res.* **2021**, *14*, 1961-1966.

(56) Mark, P.; Helfrich, W. Space-Charge-Limited Currents in Organic Crystals. *J. Appl. Phys.* **1962**, *33*, 205-215.

(57) Sangwan, V. K.; Rangnekar, S. V.; Kang, J.; Shen, J.; Lee, H.-S.; Lam, D.; Shen, J.; Liu, X.; de Moraes, A. C. M.; Kuo, L.; Gu, J.; Wang, H.; Hersam, M. C. Visualizing Thermally Activated Memristive Switching in Percolating Networks of Solution-Processed 2D Semiconductors. *Adv. Funct. Mater.* **2021**, *31*, 2107385.

(58) Mott, N. F. Conduction in Non-Crystalline Materials. *Philos. Mag.* **1969**, *19*, 835-852.

TOC Graphic

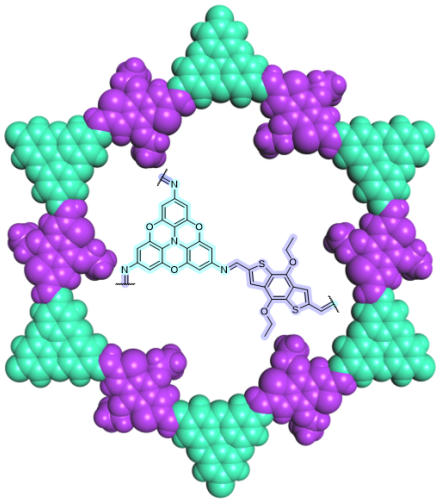

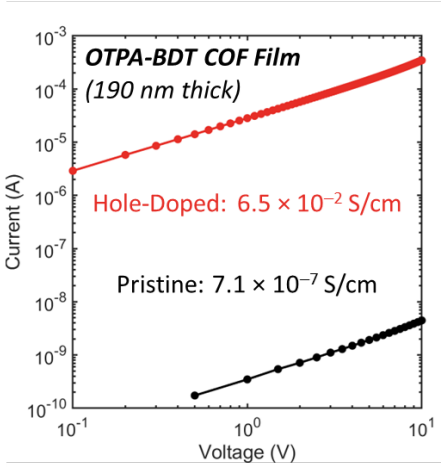
OTPA-BDT COF Film
(190 nm thick)
Hole-Doped: 6.5 × 10⁻² S/cm
Pristine: 7.1 × 10⁻⁷ S/cm
Current (A)
Voltage (V)